A Model Order Reduction Method for the Finite-Element Simulation of Inhomogeneous Waveguides

Alwin Schultschik, Ortwin Farle, and Romanus Dyczij-Edlinger

Department of Physics and Mechatronics, Lehrstuhl für Theoretische Elektrotechnik, Saarland University, Saarbrücken D-66123, Germany

A finite-element-based model order reduction method for the broadband analysis of the dominant modes of transversally inhomogeneous waveguides is presented. We show that the sub-space projections used in conventional multipoint methods may result in spurious modes in the reduced-order model and propose an improved formulation to overcome this problem. The suggested method achieves error levels comparable to those of the underlying finite-element method, while overall solution times are significantly smaller.

***Index Terms*—Eigenvalue problems, electromagnetic fields, finite-element methods (FEMs), model order reduction.**

I. Introduction

THE EVER increasing operating frequencies of both digital and analog systems have raised the need for the accurate prediction of propagation characteristics and modal field patterns of wave guiding structures over wide frequency bands. Since the waveguides considered are typically characterized by cross-sections of complicated geometry and inhomogeneous material properties, analytical solutions are usually not available. Among the numerical tools available, the finite-element (FE) method [1], [2] stands out for its high flexibility and accuracy. However, conventional FE analysis over wide frequency bands tends to be time-consuming, because large-scale eigenvalue problems are to be solved at a great number of frequency points. To overcome this problem, several approaches to fast frequency sweep computations have been proposed. In [3] and [4], single point methods based on asymptotic waveform evaluation were presented. The multipoint method of [5] constructs a reduced order model (ROM) by projecting the underlying FE system to a low-dimensional sub-space spanned by modal field patterns computed at selected expansion points.

In this paper, we numerically demonstrate the appearance of spurious modes in conventional projection-type ROMs, explain their origin, and propose a new method to overcome this deficiency.

II. FE Formulation and Null-Fields

The waveguides considered are source-free, inhomogeneous in the transverse plane but uniform along the axis, and bounded by perfect electric and magnetic conductors. For the potential formulation, uniformity along the z-axis allows to express the magnetic vector potential $\vec{A}$ and the electric scalar potential φ as

$$\vec{A} = e^{-\gamma z}(\vec{A}_t\,(x,y) + A_z(x,y)\hat{e}_z) \tag{1}$$

$$\varphi = e^{-\gamma z}V(x,y) \tag{2}$$

where $\gamma = \alpha + j\beta$ stands for the propagation constant, subscript t for transversal components, and $\hat{e}_z$ for the unit vector in z direction. For increased numerical robustness [2], we split the transverse vector potential $\vec{A}_t\,(x,y)$ into a transverse gradient $\nabla_t\psi$ plus a function $\vec{A}_t^{\,c}\,(x,y)$ of non-vanishing circulation

$$\vec{A}_t\,(x,y) = \vec{A}_t^{\,c}\,(x,y) + \nabla_t\psi(x,y) \tag{3}$$

and apply the axial gauge $A_z \equiv 0$. FE discretization results in a p dimensional algebraic eigenvalue problem of the form

$$(\mathbf{S}_0 + k\mathbf{S}_1 + k^2\mathbf{S}_2)\mathbf{v} - \gamma^2\mathbf{T}\mathbf{v} = \mathbf{0} \text{ with } \quad \mathbf{v} = \begin{bmatrix}\mathbf{v}_A\\ \mathbf{v}_\psi\\ \mathbf{v}_V\end{bmatrix} \tag{4}$$

where $\mathbf{v}_A, \mathbf{v}_\psi$, and $\mathbf{v}_V$ denote the component vectors of $\vec{A}_t^{\,c}, \psi$, and V, and the matrices $\mathbf{S}_0, \mathbf{S}_1, \mathbf{S}_2$, and $\mathbf{T}$ are given by

$$\mathbf{S}_0 = \begin{bmatrix}\mathbf{S}^{\nu}_{AA} & \mathbf{0} & \mathbf{0}\\ \mathbf{0} & \mathbf{0} & \mathbf{0}\\ \mathbf{0} & \mathbf{0} & -\mathbf{S}^{\varepsilon}_{VV}\end{bmatrix} \quad \mathbf{S}_1 = \begin{bmatrix}\mathbf{0} & \mathbf{0} & \mathbf{C}^{\varepsilon}_{AV}\\ \mathbf{0} & \mathbf{0} & \mathbf{S}^{\varepsilon}_{VV}\\ \mathbf{C}^{\varepsilon T}_{AV} & \mathbf{S}^{\varepsilon T}_{VV} & \mathbf{0}\end{bmatrix}$$

$$\mathbf{S}_2 = -\begin{bmatrix}\mathbf{T}^{\varepsilon}_{AA} & \mathbf{C}^{\varepsilon}_{AV} & \mathbf{0}\\ \mathbf{C}^{\varepsilon T}_{AV} & \mathbf{S}^{\varepsilon}_{VV} & \mathbf{0}\\ \mathbf{0} & \mathbf{0} & \mathbf{0}\end{bmatrix} \quad \mathbf{T} = \begin{bmatrix}\mathbf{T}^{\nu}_{AA} & \mathbf{B}^{\nu}_{AV} & \mathbf{0}\\ \mathbf{B}^{\nu T}_{AV} & \mathbf{S}^{\nu}_{VV} & \mathbf{0}\\ \mathbf{0} & \mathbf{0} & -\mathbf{T}^{\varepsilon}_{VV}\end{bmatrix}. \tag{5}$$

We employ the hierarchical basis functions of [6]. By denoting scalar and vector basis functions by $W \in H^1$ and $\vec{w} \in H(\mathrm{curl})$, respectively, above submatrices are given by

$$[S^{\nu}_{AA}]_{ik} = \int \nabla_t \times \vec{w}_i \cdot \mu_r^{-1}\nabla_t \times \vec{w}_k d\Omega \tag{6}$$

$$[T^{\varepsilon}_{AA}]_{ik} = \int \vec{w}_i \cdot \varepsilon_r \vec{w}_k d\Omega \tag{7}$$

$$[C^{\varepsilon}_{AV}]_{ik} = \int \vec{w}_i \cdot \varepsilon_r \nabla_t W_k d\Omega \tag{8}$$

$$[S^{\varepsilon}_{VV}]_{ik} = \int \nabla_t W_i \cdot \varepsilon_r \nabla_t W_k d\Omega \tag{9}$$

$$[S^{\nu}_{VV}]_{ik} = \int \nabla_t W_i \cdot \mu_r^{-1}\nabla_t W_k d\Omega \tag{10}$$

$$[B^{\nu}_{AV}]_{ik} = \int \vec{w}_i \cdot \mu_r^{-1}\nabla_t W_k d\Omega \tag{11}$$

$$[T^{\nu}_{AA}]_{ik} = \int \vec{w}_i \cdot \mu_r^{-1}\vec{w}_k d\Omega \tag{12}$$

$$[T^{\varepsilon}_{VV}]_{ik} = \int W_i \varepsilon_r W_k d\Omega. \tag{13}$$

Note that (4) supports null-field solutions $\mathbf{n}$ [2] of the form

$$\mathbf{n} \in \mathrm{Ran}(\mathbf{V}_I), \text{where } \mathbf{V}_I^T = [\,\mathbf{0} \quad \mathbf{I} \quad k\mathbf{I}\,]. \tag{14}$$

Digital Object Identifier 10.1109/TMAG.2007.915800

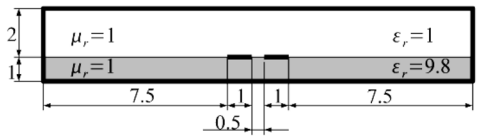

Fig. 1. Geometry of shielded microstrip transmission line. All dimensions are in millimeters. Signal lines are modelled as infinitely thin perfect conductors.

III. Model Order Reduction

Conventional multipoint methods build a matrix $\mathbf{V}$ from the first m eigenvectors $\mathbf{v}_i$ of (4) at n expansion points k_j

$$\mathbf{V} = [\mathbf{v}_1(k_1), \ldots, \mathbf{v}_m(k_1), \mathbf{v}_1(k_2), \ldots, \mathbf{v}_m(k_n)] \tag{15}$$

and restrict (4) to the subspace $\mathrm{Ran}(\mathbf{V})$. For numerical stability, $\mathbf{V}$ is $\mathbf{QR}$ factorized, and the unitary matrix $\mathbf{Q}$ serves as the projection matrix in a structure-preserving Galerkin process [5] applied to the original problem (4), (5). The resulting ROM is of very small dimension $q = m \cdot n \ll p$ and takes the form

$$(\tilde{\mathbf{S}}_0 + k\tilde{\mathbf{S}}_1 + k^2\tilde{\mathbf{S}}_2)\tilde{\mathbf{v}} - \tilde{\gamma}^2\tilde{\mathbf{T}}\tilde{\mathbf{v}} = \mathbf{0} \tag{16}$$

where

$$\tilde{\mathbf{S}}_0 = \mathbf{Q}^H\mathbf{S}_0\mathbf{Q}, \quad \tilde{\mathbf{S}}_1 = \mathbf{Q}^H\mathbf{S}_1\mathbf{Q}, \quad \tilde{\mathbf{S}}_2 = \mathbf{Q}^H\mathbf{S}_2\mathbf{Q} \tag{17}$$

$$\tilde{\mathbf{T}} = \mathbf{Q}^H\mathbf{T}\mathbf{Q}, \quad \mathbf{v} = \mathbf{Q}\tilde{\mathbf{v}}. \tag{18}$$

Fig. 2(a) presents a fast frequency sweep for the waveguide of Fig. 1, using $m = 6$ and $n = 3$. While the sought $m = 6$ dominant modes are approximated well, the remaining $m(n-1) = 12$ waveforms are superpositions of null-fields and physical modes of higher order, and some of them clearly exhibit non-physical behavior: they even propagate in the static limit. The field formulation [1] exhibits similar behavior.

IV. Spurious Solutions

A. Non-Physical Solutions in the Static Limit

To clarify the origin of such non-physical solutions, we investigate the lossless case in the static limit, $k = 0$. For the non-reduced problem (4), the abbreviations

$$\mathbf{v}_{A\psi} = \begin{bmatrix} \mathbf{v}_A \\ \mathbf{v}_\psi \end{bmatrix}, \quad \mathbf{S}^\nu_{A\psi} = \begin{bmatrix} \mathbf{S}^\nu_{AA} & \mathbf{0} \\ \mathbf{0} & \mathbf{0} \end{bmatrix}, \quad \mathbf{T}^\nu_{A\psi} = \begin{bmatrix} \mathbf{T}^\nu_{AA} & \mathbf{B}^\nu_{AV} \\ \mathbf{B}^{\nu T}_{AV} & \mathbf{S}^\nu_{VV} \end{bmatrix} \tag{19}$$

yield the simpler form

$$\left(\begin{bmatrix} \mathbf{S}^\nu_{A\psi} & \mathbf{0} \\ \mathbf{0} & -\mathbf{S}^\varepsilon_{VV} \end{bmatrix} - \gamma^2 \begin{bmatrix} \mathbf{T}^\nu_{A\psi} & \mathbf{0} \\ \mathbf{0} & -\mathbf{T}^\varepsilon_{VV} \end{bmatrix} \right) \begin{bmatrix} \mathbf{v}_{A\psi} \\ \mathbf{v}_V \end{bmatrix} = \mathbf{0}. \tag{20}$$

Note that the $A\psi$ and V components are decoupled. Since $\mathbf{S}^\nu_{A\psi}$ is positive semi-definite, and $\mathbf{S}^\varepsilon_{VV}$, $\mathbf{T}^\nu_{A\psi}$, and $\mathbf{T}^\varepsilon_{VV}$ are positive definite, all eigenvalues of the original eigenvalue problem are real-valued and non-negative, $\gamma^2 \geq 0$. On the other hand, the projection matrix $\mathbf{Q}$ does not maintain separate degrees of freedom for $A\psi$ and V components in the ROM. Therefore, the decoupled structure gets lost, and the relevant reduced order matrices are given by

$$\tilde{\mathbf{S}}_0 = \mathbf{Q}^H_{A\psi}\mathbf{S}^\nu_{A\psi}\mathbf{Q}_{A\psi} - \mathbf{Q}^H_V\mathbf{S}^\varepsilon_{VV}\mathbf{Q}_V \tag{21}$$

$$\tilde{\mathbf{T}} = \mathbf{Q}^H_{A\psi}\mathbf{T}^\nu_{A\psi}\mathbf{Q}_{A\psi} - \mathbf{Q}^H_V\mathbf{T}^\varepsilon_{VV}\mathbf{Q}_V \tag{22}$$

where

$$\mathbf{Q}^H = \begin{bmatrix} \mathbf{Q}^H_A & \mathbf{Q}^H_\psi & \mathbf{Q}^H_V \end{bmatrix}, \quad \mathbf{Q}^H_{A\psi} = \begin{bmatrix} \mathbf{Q}^H_A & \mathbf{Q}^H_\psi \end{bmatrix}. \tag{23}$$

Since both $\tilde{\mathbf{S}}_0$ and $\tilde{\mathbf{T}}$ are given by differences of (semi-)definite matrices, they may become indefinite, and the static limit of the ROM, $(\tilde{\mathbf{S}}_0 - \tilde{\gamma}^2\tilde{\mathbf{T}})\tilde{\mathbf{v}} = \mathbf{0}$, may possess negative or even complex eigenvalues $\tilde{\gamma}^2$.

One way of preserving separate variables for $A\psi$ and V in the ROM is to choose the projection matrix

$$\mathbf{Q}' = \begin{bmatrix} \mathbf{Q}_{A\psi} & \mathbf{0} \\ \mathbf{0} & \mathbf{Q}_V \end{bmatrix}. \tag{24}$$

However, this procedure doubles the dimension of the ROM and introduces null-field solutions (14).

Our preferred resolution is to multiply the second row of (20), i.e., the third row of the original problem (4) and (5), by -1, so that the relevant matrices read

$$\tilde{\mathbf{S}}_0 = \mathbf{Q}^H_{A\psi}\mathbf{S}^\nu_{A\psi}\mathbf{Q}_{A\psi} + \mathbf{Q}^H_V\mathbf{S}^\varepsilon_{VV}\mathbf{Q}_V \tag{25}$$

$$\tilde{\mathbf{T}} = \mathbf{Q}^H_{A\psi}\mathbf{T}^\nu_{A\psi}\mathbf{Q}_{A\psi} + \mathbf{Q}^H_V\mathbf{T}^\varepsilon_{VV}\mathbf{Q}_V. \tag{26}$$

Now, $\tilde{\mathbf{S}}_0$ is positive semi-definite, and $\tilde{\mathbf{T}}$ is positive definite, and all eigenvalues remain real-valued and non-negative, $\tilde{\gamma}^2 \geq 0$. Fig. 2(b) illustrates the elimination of propagating modes in the static limit. Nevertheless, there are still spurious modes in the spectral range of the sought modes, which are superposition of null-fields and physical modes of higher order.

B. Null-Field Orthogonalization

At any chosen wave number k, all physical eigenmodes $\mathbf{v}$ of (4) satisfy the orthogonality relation [2], [3]

$$\mathbf{V}^T_I(k)\mathbf{T}\mathbf{v}(k) = \mathbf{0}. \tag{27}$$

Nevertheless, we may have $\mathbf{V}^T_I(k)\mathbf{T}\mathbf{Q} \neq \mathbf{0}$ almost everywhere, because $\mathbf{Q}$ is constructed from eigenvectors at *a finite number* of expansion points, and the considered wave number may differ from each of them. Hence, away from expansion points, the basis vectors for the ROM are composed of both physical and null-field components. To resolve this situation, we exploit the fact that the subvector $\mathbf{v}_\psi$ can be determined from $\mathbf{v}_A$ and $\mathbf{v}_V$ by means of the orthogonality relation (27)

$$\mathbf{v}_\psi(k) = k\mathbf{S}^{\nu,-1}_{VV}\mathbf{T}^\varepsilon_{VV}\mathbf{v}_V(k) - \mathbf{S}^{\nu,-1}_{VV}\mathbf{B}^{\nu T}_{AV}\mathbf{v}_A(k). \tag{28}$$

This enables us to construct a wave-number-dependent projection matrix $\mathbf{Q}_k(k) = \mathbf{Q}_0 + k\mathbf{Q}_1$ with

$$\mathbf{Q}_0 = \begin{bmatrix} \mathbf{Q}_A \\ -\mathbf{S}^{\nu,-1}_{VV}\mathbf{B}^{\nu T}_{AV}\mathbf{Q}_A \\ \mathbf{Q}_V \end{bmatrix} \quad \mathbf{Q}_1 = \begin{bmatrix} \mathbf{0} \\ \mathbf{S}^{\nu,-1}_{VV}\mathbf{T}^\varepsilon_{VV}\mathbf{Q}_V \\ \mathbf{0} \end{bmatrix} \tag{29}$$

which ensures $\mathbf{T}$ orthogonality (27) at any wave number and thus eliminates null-field components from the ROM. Fig. 2(c) shows that the sole application of null-field orthogonalization does not eliminate non-physical solutions in the static limit.

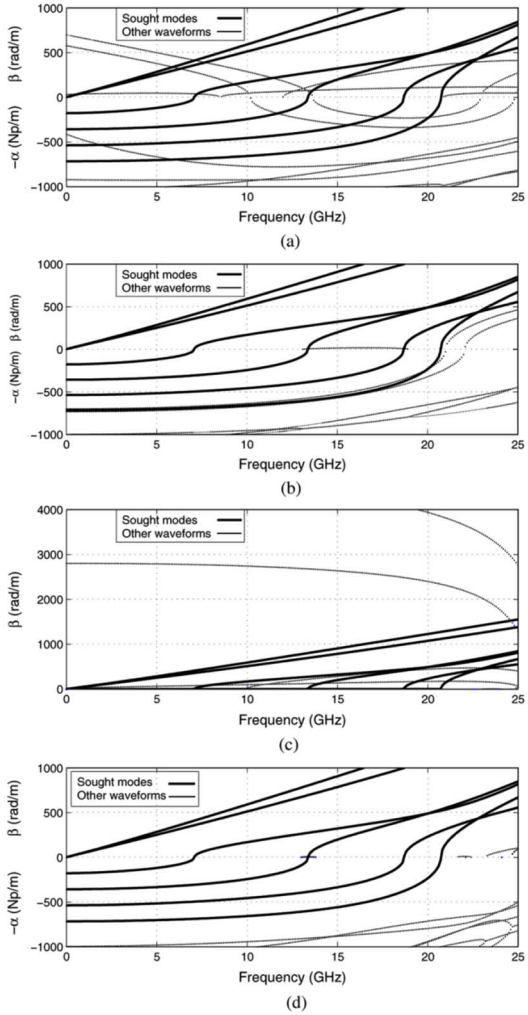

Fig. 2. Dispersion characteristics for microstrip line of Fig. 1 and second-order elements. Reduction based on six modes at 0, 10, and 20 GHz. (a) Conventional ROM, exhibiting spurious modes. (b) Modified ROM, eliminating propagable modes in static limit. (c) ROM with null-field orthogonalization only. (d) Proposed ROM.

V. Proposed ROM

By applying $\mathbf{Q}_k(k)$ as the projection matrix and collecting equal powers of k, we arrive at the eigenvalue problem

$$(\tilde{\mathbf{S}}_{S0} + k\tilde{\mathbf{S}}_{S1} + k^2\tilde{\mathbf{S}}_{S2} + k^3\tilde{\mathbf{S}}_{S3} + k^4\tilde{\mathbf{S}}_{S4})\tilde{\mathbf{v}} - \tilde{\gamma}^2(\tilde{\mathbf{T}}_{T0} + k\tilde{\mathbf{T}}_{T1} + k^2\tilde{\mathbf{T}}_{T2})\tilde{\mathbf{v}} = \mathbf{0} \quad (30)$$

where

$$\tilde{\mathbf{S}}_{S1} = \tilde{\mathbf{S}}_{100} + \tilde{\mathbf{S}}_{010} + \tilde{\mathbf{S}}_{001}, \quad \tilde{\mathbf{S}}_{S0} = \tilde{\mathbf{S}}_{000} \quad (31)$$

$$\tilde{\mathbf{S}}_{S2} = \tilde{\mathbf{S}}_{110} + \tilde{\mathbf{S}}_{011} + \tilde{\mathbf{S}}_{101} + \tilde{\mathbf{S}}_{020} \quad (32)$$

$$\tilde{\mathbf{S}}_{S3} = \tilde{\mathbf{S}}_{111} + \tilde{\mathbf{S}}_{120} + \tilde{\mathbf{S}}_{021}, \quad \tilde{\mathbf{S}}_{S4} = \tilde{\mathbf{S}}_{121} \quad (33)$$

$$\tilde{\mathbf{T}}_{T0} = \tilde{\mathbf{T}}_{00}, \quad \tilde{\mathbf{T}}_{T1} = \tilde{\mathbf{T}}_{10} + \tilde{\mathbf{T}}_{01}, \quad \tilde{\mathbf{T}}_{T2} = \tilde{\mathbf{T}}_{11} \quad (34)$$

$$\tilde{\mathbf{S}}_{ijk} = \mathbf{Q}_i^H\bar{\mathbf{S}}_j\mathbf{Q}_k, \quad \tilde{\mathbf{T}}_{ik} = \mathbf{Q}_i^H\bar{\mathbf{T}}\mathbf{Q}_k. \quad (35)$$

Here, $\bar{\mathbf{S}}_j$ and $\bar{\mathbf{T}}$ denote the modified matrices (5), having the third line multiplied by -1. Fig. 2(d) shows that, for the proposed ROM, there are no spurious solutions, and the curves of high order waveforms are well-separated from those of the sought modes. Note that the small phase coefficients appearing in the vicinity of 13.5 and 22 GHz as well as above 23 GHz belong to high order complex modes with large attenuation coefficients.

TABLE I
Computational Parameters and Runtime Comparisons

Example	A	B	C	C (lossy)
Parameters:				
Unknowns	5991	10671	9905	9905
Frequency range (GHz)	0 to 25	0 to 25	0 to 18	0 to 18
Step width (MHz)	100	100	100	100
Evaluation points	251	251	181	181
Modes	6	7	8	8
Expansion points	6	6	7	7
Order of FE basis	2	2	3	3
Runtimes:				
Full FE solver (s)	1018	1878	1075	1993
ROM generation (s)	65	129	145	185
ROM evaluation (s)	0.6	2.4	4.0	4.0

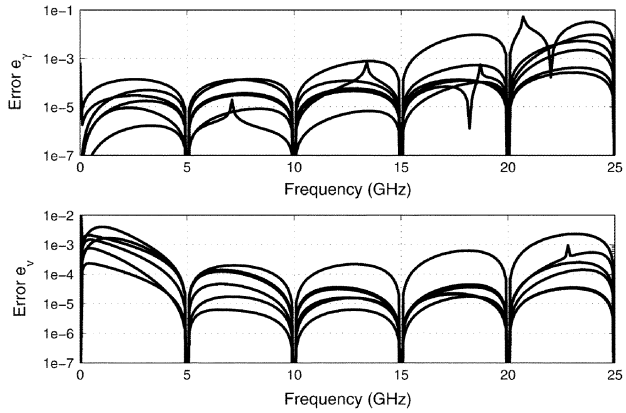

Fig. 3. Error plots for shielded microstrip line of Example A.

VI. Numerical Results

To compare the accuracy of the ROM to that of the original problem, both eigenvalues and eigenvectors are considered. For a given mode i, the errors in eigenvalue e_{γ_i} and eigenvector e_{v_i} are defined by

$$e_{\gamma_i} = |\gamma_i - \tilde{\gamma}_i| \quad (36)$$

$$e_{v_i} = \left\| \frac{\mathbf{v}_i}{\|\mathbf{v}_i\|_2} - \frac{\mathbf{Q}_k(k)\tilde{\mathbf{v}}_i}{\|\mathbf{Q}_k(k)\tilde{\mathbf{v}}_i\|_2} \right\|_2. \quad (37)$$

Runtime comparisons with full FE runs are given in Table I.

The following experiments show that the proposed method achieves error levels comparable to those of the underlying FE method, while overall solution times are significantly smaller.

A. Shielded Microstrip Line 1

To complete the investigation of the example given in Fig. 1, computational parameters and error plots are presented in Table I-A and Fig. 3, respectively.

B. Shielded Microstrip Line 2

Our next example, the microstrip line of Fig. 4, was also considered in [4], [5], and [7]. This structure supports complex modes in the considered frequency band from 0 to 25 GHz, where the first seven even modes are computed. From the point of view of model reduction, the main difference to the previous example is the presence of complex matrices in the ROM, even without losses in the structure. Our results are given in Table I-B and Fig. 5.

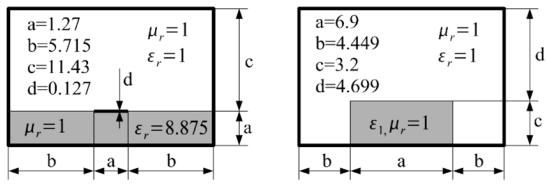

Fig. 4. Shielded microstrip line (left) and dielectric-loaded waveguide (right). All dimensions are in millimeters. Figures are not in scale.

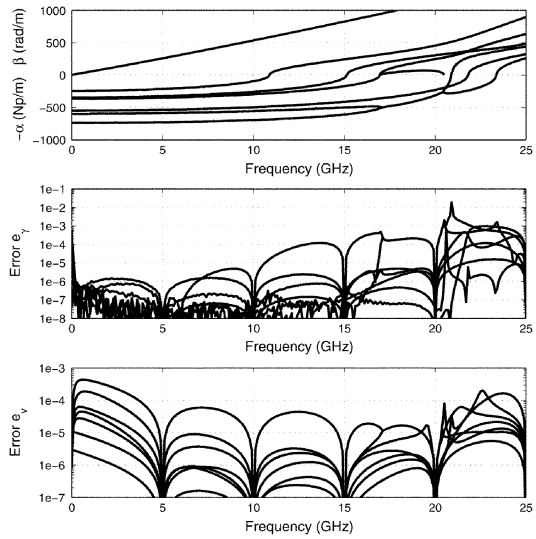

Fig. 5. Dispersion characteristics and error plots for Example B.

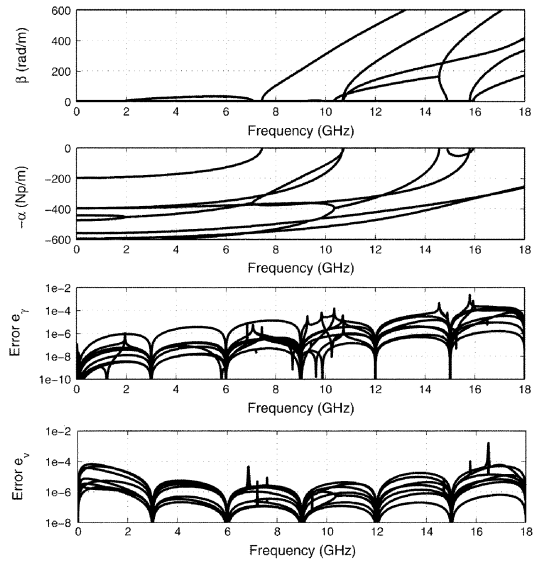

Fig. 6. Dispersion characteristics and error plots for Example C.

C. Dielectric-Loaded Waveguide

Fig. 4 shows a dielectric-loaded waveguide. For the permittivity chosen, $\varepsilon_1 = 9\varepsilon_0$, the structure supports complex modes and even backward waves [8]. Fig. 6 shows dispersion characteristics and errors and Table I-C presents computational parameters and timing. To demonstrate the ability of the proposed technique to handle losses, we set the permittivity to $\varepsilon_1 = \varepsilon_0(9 - j0.1)$ and investigate the bifurcation at 14.5 GHz. Our results are shown in Fig. 7.

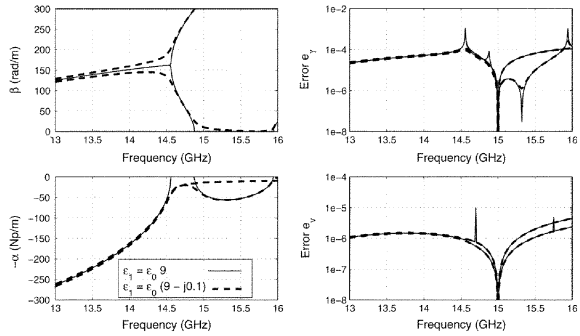

Fig. 7. Complex modes with and without losses, Example C.

VII. Conclusion

We have demonstrated the appearance of spurious modes in conventional multipoint methods of model order reduction. Such waveforms are given by superpositions of higher order physical modes and null-fields of the original problem, and some of them even propagate in the static limit.

The proposed method overcomes these deficiencies by manipulating the matrices of the original system and introducing frequency-dependent projection matrices that render the reduced order subspace orthogonal to null-fields. The resulting algorithm is fast and reliable. In the future, we shall determine the model order automatically.

Acknowledgment

This work was supported in part by Ansoft Corporation.

References

[1] J.-F. Lee, D.-K. Sun, and Z. J. Cendes, "Full-wave analysis of dielectric waveguides using tangential vector finite elements," *IEEE Trans. Microw. Theory Tech.*, vol. 39, no. 8, pp. 1262–1271, Aug. 1991.

[2] O. Farle, V. Hill, and R. Dyczij-Edlinger, "Finite-element waveguide solvers revisited," *IEEE Trans. Magn.*, vol. 40, no. 2, pp. 1468–1471, Mar. 2004.

[3] S. V. Polstyanko, R. Dyczij-Edlinger, and J.-F. Lee, "Fast frequency sweep technique for the efficient analysis of dielectric waveguides," *IEEE Trans. Microw. Theory Tech.*, vol. 45, no. 7, pp. 1118–1126, Jul. 1997.

[4] S.-H. Lee, T.-Y. Huang, and R.-B. Wu, "Fast waveguide eigenanalysis by wide-band finite-element model-order reduction," *IEEE Trans. Microw. Theory Tech.*, vol. 53, no. 8, pp. 2552–2558, Aug. 2005.

[5] F. Bertazzi, O. Peverini, M. Goano, G. Ghione, R. Orta, and R. Tascone, "A fast reduced-order model for the full-wave FEM analysis of lossy inhomogeneous anisotropic waveguides," *IEEE Trans. Microw. Theory Tech.*, vol. 50, no. 9, pp. 2108–2114, Sep. 2002.

[6] P. Ingelström, "A new set of h(curl)-conforming hierarchical basis functions for tetrahedral meshes," *IEEE Trans. Microw. Theory Tech.*, vol. 54, no. 1, pp. 106–114, Jan. 2006.

[7] L. Valor and J. Zapata, "Efficient finite element analysis of waveguides with lossy inhomogeneous anisotropic materials characterized by arbitrary permittivity and permeability tensors," *IEEE Trans. Microw. Theory Tech.*, vol. 43, no. 10, pp. 2452–2459, Oct. 1995.

[8] J. Strube and F. Arndt, "Rigorous hybrid-mode analysis of the transition from rectangular waveguide to shielded dielectric image guide," *IEEE Trans. Microw. Theory Tech.*, vol. 33, no. 5, pp. 391–401, May 1985.

Manuscript received June 24, 2007. Corresponding author: A. Schultschik (e-mail: a.schultschik@lte.uni-saarland.de).